



1 **Mapping Paddy Rice Distribution and Cropping Intensity in
2 South and Southeast Asia (1995 - 2024) at 30m Resolution**

3 Zizhang Zhao^{1,2}, Geli Zhang^{1*}, Jinwei Dong^{2,3}, Jilin Yang⁴, Xiangming Xiao⁵

4 1 College of Land Science and Technology, China Agricultural University, Beijing 100193, China

5 2 Institute of Geographic Sciences and Natural Resources Research, Chinese Academy of Sciences, Beijing
6 100101, China

7 3 University of Chinese Academy of Sciences, Beijing 100049, China

8 4 College of Grassland Science and Technology, China Agricultural University, Beijing 100193, China

9 5 School of Biological Sciences, University of Oklahoma, Norman, OK 73019, USA

10 *Correspondence to:* Geli Zhang (geli.zhang@cau.edu.cn)



11 **Abstract:** South and Southeast Asia, a major global hub for paddy rice cultivation, exhibits the highest rice
12 cropping intensity worldwide due to its favourable hydrothermal conditions, and also has experienced considerable
13 spatiotemporal changes due to climate change and anthropogenic activities. However, the absence of long-term
14 spatial distribution and cropping intensity of paddy rice hinders effective agricultural and environmental
15 management. This gap is particularly critical especially in the 21st century, with enhanced impacts from changing
16 climate, water resources, and food trade pattern. Using all the available Landsat and Sentinel-2 archives, we refined
17 a phenology-based algorithm to generate 30-m rice maps and cropping intensity across South and Southeast Asia
18 for the years 1995, 2005, 2015, and 2024. The algorithm overcomes the challenge of detecting rice cropping
19 intensity in long time-series and comprises three core steps: (1) identifying pixel-level rice phenological peaks
20 using an enhanced peak detection method, thereby defining potential transplanting windows and minimizing
21 monsoon-induced cloud and precipitation interference; (2) detecting paddy flooding signals and delineating rice
22 cultivation areas based on phenological rules derived from the relationship between the Land Surface Water Index
23 (LSWI) and Enhanced Vegetation Index (EVI); (3) determining rice cropping intensity according to the number
24 of valid crop peaks and associated flooding signals within a single year. The resulting maps were validated using
25 23,396 samples collectively derived from a field photo library, visual interpretation of Sentinel-1/2 satellite
26 imagery, and a sample migration algorithm. Across the four periods, the maps achieved overall accuracies ranging
27 from 83% to 87%. In addition, the resultant products were compared with existing regional and period-specific
28 rice datasets (e.g., NESEA-RICE10 and Open-SEA-Rice-10) for further evaluation. The comparisons
29 demonstrated that the refined approach achieved higher accuracy and robustness in mapping both rice distribution
30 and cropping intensity, whereas the existing products performed well only in partial environments. When
31 compared with the FAO official statistics for South and mainland Southeast Asian countries, the derived maps
32 yielded R^2 values exceeding 0.9. This dataset holds great potential for applications such as methane emission



33 estimation, water resource management, and crop yield monitoring, thereby supporting sustainable agricultural
34 practices and policy development in the region.



35 **1. Introduction**

36 Rice is a staple food crop across South and Southeast Asia, underpinning food security in a region characterized
37 by rapid population growth and escalating food demand (Xiao et al., 2006). This demographic pressure has
38 inevitably driven the expansion of rice paddies and intensified cultivation practices (Godfray et al., 2010; Foley et
39 al., 2005). However, the expansion of agricultural land, including rice paddies, exacerbates environmental
40 challenges, such as freshwater depletion, deforestation, and increased methane emissions, all of which threaten
41 ecosystem functions (Mehta et al., 2024; Wang et al., 2023; Zeng et al., 2018; Chen et al., 2024). Balancing food
42 security with the preservation of ecosystem services is thus a critical component of achieving the United Nations'
43 2030 Sustainable Development Goals (SDGs) (Persaud and Dagher, 2021). Understanding the spatial extent and
44 cropping intensification patterns of rice agriculture is essential to provide robust data support for sustainable
45 development policies (Potapov et al., 2022; Zabel et al., 2019).

46 Satellite remote sensing has emerged as a powerful tool for accurately mapping rice agriculture over large spatial
47 scales (Dong and Xiao, 2016; Zhang et al., 2017). Moderate Resolution Imaging Spectroradiometer (MODIS) data,
48 with its 500-meter spatial resolution, has been effectively utilized to map rice distributions in monsoon Asia,
49 including South and Southeast Asia (Zhang et al., 2020). However, the coarse resolution of MODIS limits its
50 ability to capture fragmented rice paddies and introduces errors due to mixed-pixel effects, particularly in detecting
51 multi-cropping systems (Han et al., 2021). Higher-resolution satellite data, such as those from Landsat (30 m) and
52 Sentinel (10–20 m), enable more precise identification of rice paddies (Zhao et al., 2024). Current research
53 employs phenology-based algorithms or machine learning approaches to leverage these higher-resolution datasets
54 for rice mapping.

55 Phenology-based rice mapping methods primarily exploit the relationship between the Land Surface Water Index
56 (LSWI) and the Enhanced Vegetation Index (EVI) derived from optical imagery to detect the unique flooding
57 signals of rice paddies (Dong et al., 2015; Xiao et al., 2005). These methods have achieved high accuracy in regions
58 such as Northeast China, Japan, and South Korea (Dong et al., 2016; Carrasco et al., 2022; Han et al., 2022).
59 Recent studies have extended phenology-based approaches to Synthetic Aperture Radar (SAR) data, improving
60 rice mapping in cloud-prone and rainy regions (Xu et al., 2023; Song et al., 2025). Due to their simplicity,
61 computational efficiency, and robustness, phenology-based methods are particularly well-suited for large-scale
62 applications and can be readily implemented on cloud-computing platforms, making them the most widely adopted
63 approach for regional and continental-scale rice mapping studies (Zhao et al., 2025a).



64 Machine learning-based rice classification methods have also gained prominence, as they leverage extensive
65 training samples to achieve high accuracy in mapping paddy rice distribution (Dong and Xiao, 2016). For instance,
66 several studies have achieved high-precision rice mapping in regions with complex cropping patterns, such as the
67 crop rotation systems in Northeast China and the multi-season rice planting patterns in the Jianghan Plain, by
68 integrating rice-specific phenological features with machine learning classifiers, such as One-Class Support Vector
69 Machines (OC-SVM) and Random Forest (He et al., 2021; Ni et al., 2021). More recently, deep learning techniques,
70 particularly convolutional neural networks like U-Net and eXplainable Mamba UNet, have been employed to
71 process time-series Sentinel-1 SAR data, demonstrating remarkable robustness in capturing spatial patterns, even
72 in cloud-prone regions where optical imagery is limited (Ge et al., 2025; Thorp and Drajat, 2021; Lin et al., 2022).
73 Despite the achievements of the above two mapping approaches, none has yet provided a method capable of long-
74 term, large-scale analysis with precise extraction of cropping intensity and spatial distribution to elucidate the
75 spatiotemporal patterns of rice distribution in South and Southeast Asia. Traditional phenology-based rice mapping
76 methods rely on prior expert knowledge to determine phenological stages, but interpreting phenological periods
77 from several decades ago introduces considerable uncertainty. Machine learning methods, on the other hand, have
78 shown potential for global-scale classification, yet the acquisition of large, high-quality historical training datasets
79 remains time-consuming and resource-intensive (Zhan et al., 2021). Even though a fully automated, sample-free
80 rice-mapping framework has been developed, its dependence on SAR-derived rice features limits its applicability
81 to periods beyond the operational lifetime of Sentinel-1 (Gao et al., 2023).
82 This study addresses this gap by employing a refined phenology-based method that eliminates the need for
83 extensive training samples while accurately identifying planting intensity and phenological windows. Through
84 optical imagery fusion and false peak elimination techniques, we aim to precisely identify rice cropping systems
85 and their spatial distributions, while quantifying changes over the past three decades. This approach provides
86 critical data to reconcile the conflict between traditional rice cultivation expansion and sustainable development
87 goals, offering robust support for informed policy-making in South and mainland Southeast Asia.

88 **2. Materials**

89 **2.1 Study area**

90 The study area encompasses South and mainland Southeast Asia countries, specifically Vietnam, Thailand,
91 Cambodia, Myanmar, Laos, Bangladesh, India, and Pakistan (Fig. S1). These eight countries are predominantly



92 characterized by a tropical monsoon climate (with the exception of Balochistan Province), featuring distinct wet
93 and dry seasons. Rice is the predominant crop in this region, with the highest cropping intensity globally. In 2024,
94 the total rice harvested area in this region accounted for approximately 47% of the global rice harvested area,
95 making it the world's most critical rice production base.

96 **2.2 Data and preprocessing**

97 **2.2.1 Satellite imagery**

98 To develop long-term rice mapping products for South and mainland Southeast Asia, we acquired all available
99 Sentinel-2 (S2_HARMONIZED) and Landsat T1_L2 imagery data from the Google Earth Engine (GEE) platform
100 for specific time periods (Table 1). Invalid observations, including clouds, cloud shadows, and snow cover, were
101 filtered out using the Sentinel-2 QA60 and Landsat QA_PIXEL bands. However, because imagery from a single
102 year was insufficient to reliably support rice information extraction across South and mainland Southeast Asia, we
103 applied a multi-year median compositing approach for the periods 1993–1997, 2003–2007, 2014–2016, and 2023–
104 2025 to mitigate data gaps (see Table 1). Specifically, each year was segmented into half-monthly intervals (e.g.,
105 January 1–15 and January 16–31, with some intervals spanning 14 or 16 days due to monthly variations), and all
106 valid observations within the selected time periods for each interval were used to generate a single median
107 composite image. Additionally, linear regression was employed to harmonize the spectral bands of Landsat and
108 Sentinel-2 data (Yang et al., 2023), resulting in the generation of half-monthly time-series curves.

109 **Table 1:** Satellite sensors and composite periods for rice mapping in South and mainland Southeast Asia

Reference Year	Satellite Sensors	Composite Period
1995	Landsat-5	1993-1997
2005	Landsat-5, -7	2003-2007
2015	Landsat-5, -7, -8	2014-2016
2022	Sentinel-2, Landsat-8	2023-2025

110
111 Based on the generated half-monthly time-series curves, we further calculated relevant vegetation indices to
112 identify the spatial distribution and cropping intensity of paddy rice, including NDVI, LSWI, and EVI (Eqs. 1–3).

113
$$NDVI = \frac{NIR - Red}{NIR + Red} \quad (1)$$

114
$$LSWI = \frac{NIR - SWIR}{NIR + SWIR} \quad (2)$$

6 / 25



115
$$EVI = 2.5 \times \frac{NIR - Red}{NIR + 6 \times Red - 7.5 \times Blue + 1} \quad (3)$$

116

117 **2.2.2 Auxiliary data**

118 **Cropland Mask.** To investigate changes in rice planting patterns in South and mainland Southeast Asia, a region
119 that has undergone significant land-use transformations, including cropland expansion and forest loss over recent
120 decades, we selected high-quality land cover and cropland products aligned with the target mapping years. Four
121 global products were chosen to mitigate uncertainties in rice mapping arising from cropland expansion. The
122 specific cropland products selected for each year are detailed in Table 2 (Zhang et al., 2021; Karra et al., 2021;
123 Potapov et al., 2022) (<https://zenodo.org/records/5571936>).

124 **Table 2:** Cropland Products Used for Cropland Mask in South and mainland Southeast Asia

Reference Year	Cropland Products
1995	GLC_FCS30 (1990, 1995)
2005	GLC_FCS30 (2005), GLAD 30 (2003)
2015	GLC_FCS30 (2015), GLAD 30 (2015)
2024	ESA (2021), GLAD (2019), ESRI (2021)

125

126 **Rice products and statistical data.** To evaluate the reliability of our mapping results, we conducted spatial
127 comparisons with several established rice mapping products, including: (1) the JAXA High-Resolution Land-Use
128 and Land-Cover Map, including the 2020 Vietnam and 2023 Southeast Asia products
129 (https://www.eorc.jaxa.jp/ALOS/en/dataset/lulc_e.htm); and (2) Li et al. (2025) and Sun et al. (2023), whose
130 datasets (NESEA-RICE10 (Han et al., 2021) and OPEN-SEA-RICE10 (Ginting et al., 2025)) focus on regional-
131 scale rice area mapping. The comparisons allowed us to assess the spatial consistency and intensity agreement
132 across products. In addition, national-level statistical data from the Food and Agriculture Organization (FAO) were
133 used to validate the mapped rice areas.

134



135 **2.3 Methodology**

136 **2.3.1 Identification of valid crop peak dates**

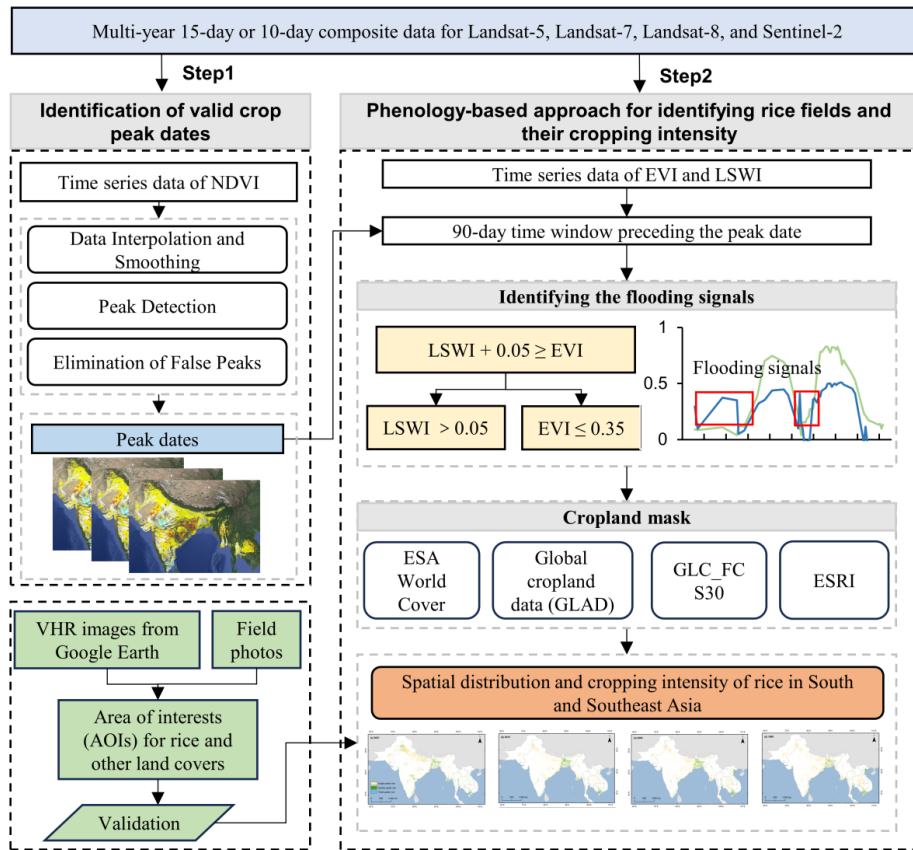
137 To accurately identify multiple rice cropping cycles, we first determined the peak date of each valid crop cycle
138 (i.e., the number of times a plot is cropped within a year). The specific steps are as follows (Fig. 1):

139 **Data Interpolation and Smoothing.** First, using the half-monthly composite imagery and derived vegetation
140 indices, NDVI outliers were removed based on the mean and three standard deviations. Linear interpolation was
141 then applied to fill gaps in the time series of LSWI and NDVI. Subsequently, the NDVI time series was smoothed
142 using the Whittaker smoothing algorithm (Whittaker Smoothing, lambda=300) to generate a smoothed time series.
143 **Peak Detection.** Peak detection was achieved by identifying local maxima and minima through iterative analysis
144 of the smoothed NDVI time-series curves. Specifically, each NDVI value was compared with its preceding value
145 to determine an increasing or decreasing trend. A point was recorded as a peak (local maximum) when the NDVI
146 transitioned from an increasing to a decreasing trend. Conversely, a point was recorded as a trough (local minimum)
147 when the NDVI shifted from a decreasing to an increasing trend.

148 **Elimination of False Peaks.** To detect and filter phenological peaks, we employed a method based on LSWI and
149 NDVI time series that identifies true phenological peaks while excluding false peaks caused by noise or non-
150 vegetation signals, thereby ensuring robust cycle detection. A complete crop growth cycle was decomposed into
151 one peak and two troughs (Yang et al., 2023). The first criterion required that the NDVI amplitude of the right
152 trough, relative to the annual maximum amplitude, exceed 35%. Second, the NDVI value at the right trough had
153 to fall below the NDVI threshold ($NDVI_{thld}$), calculated according to Eq. 5. In addition, the time span between the
154 left and right troughs had to exceed 120 days to ensure that the cycle represented a biologically reasonable rice-
155 growing season in South and mainland Southeast Asia. Each growth cycle meeting these criteria was recorded,
156 including the peak dates (day of year, DOY), while all other signals were discarded as noise.

$$NDVI_{thld} = NDVI_{min} + (NDVI_{max} - NDVI_{min}) \times 0.15 \quad (4)$$

158 Where $NDVI_{thld}$ is the NDVI threshold, $NDVI_{min}$ is the minimum NDVI value within the considered period, and
159 $NDVI_{max}$ is the maximum NDVI value within the considered period.



160

161 Figure 1. Flowchart of the mapping process for long-term rice spatial distribution and planting intensity in South
162 and mainland Southeast Asia

163 **2.3.2 Phenology-based approach for identifying rice fields and their cropping intensity**

164 The phenology-based rice mapping method identifies rice by detecting the unique biophysical characteristic of
165 fields being flooded during the transplanting period. In this study, we first selected imagery data within a 90-day
166 time window preceding the peak date of each growing season. Subsequently, flood signal detection was performed
167 on the imagery data within this time window by applying the rule $LSWI + 0.05 \geq EVI$. Notably, the LSWI and
168 EVI used here differ from those employed in crop peak identification, as these vegetation indices (VIs) do not
169 require smoothing. Additionally, to minimize interference from factors such as precipitation and soil background
170 value, we applied the rule that, when a flood signal is detected, EVI must be ≤ 0.35 and LSWI must be > 0.05 .
171 Pixels meeting these conditions were classified as rice (pixel value = 1).



172 For rice cropping intensity, we integrated multi-season rice data by calculating the number of times a pixel was
173 classified as rice (value = 1) within a year. This process generated the final rice cropping intensity distribution
174 map, with values ranging from 1 to 3, representing single-, double-, or triple-season rice, respectively.

175 **2.3.3 Accuracy assessment and comparisons**

176 Sample points for 2024 were primarily collected through visual interpretation using multiple data sources. First,
177 false-color composites of Sentinel-2 imagery (R/G/B = SWIR1, NIR, RED) representing multiple rice growth
178 stages were generated, in which rice fields during the flooded transplanting stage appeared dark green. Second,
179 following the approach of (Sun et al., 2023), we used Sentinel-1 VH time series to compute the maximum,
180 minimum, and variance values, and composed them as R: VH_max, G: VH_min, and B: VH_variance. In these
181 composites, flooded rice fields typically appeared purple, which is particularly useful for identifying rice in
182 persistently cloudy and rainy tropical regions. An example of this visualization approach has been implemented
183 and is available at the following link:

184 (<https://code.earthengine.google.com/7dd210998c6812da2e79ebcbc1536822>). Based on these two sets of
185 composites, rice sample points were manually labeled and further cross-validated using ultra-high-resolution
186 Google Earth imagery and the Global Geo-Referenced Field Photo Library (<http://www.eomf.ou.edu/photos/>). In
187 total, 4,000 rice samples were collected across the study area.

188 For the remaining 4,000 non-rice samples, random sampling was first conducted within the study area, and each
189 point was then visually verified using the same image composites to ensure the absence of rice-related features.
190 Although the above approach was effective for sample generation, manually labeling samples for periods before
191 the launch of Sentinel-1 and Sentinel-2 satellites was labor-intensive and constrained by the limited availability of
192 valid imagery. Therefore, a sample migration algorithm (Huang et al., 2020) was employed to transfer the 8,000
193 manually labeled samples to other target years.

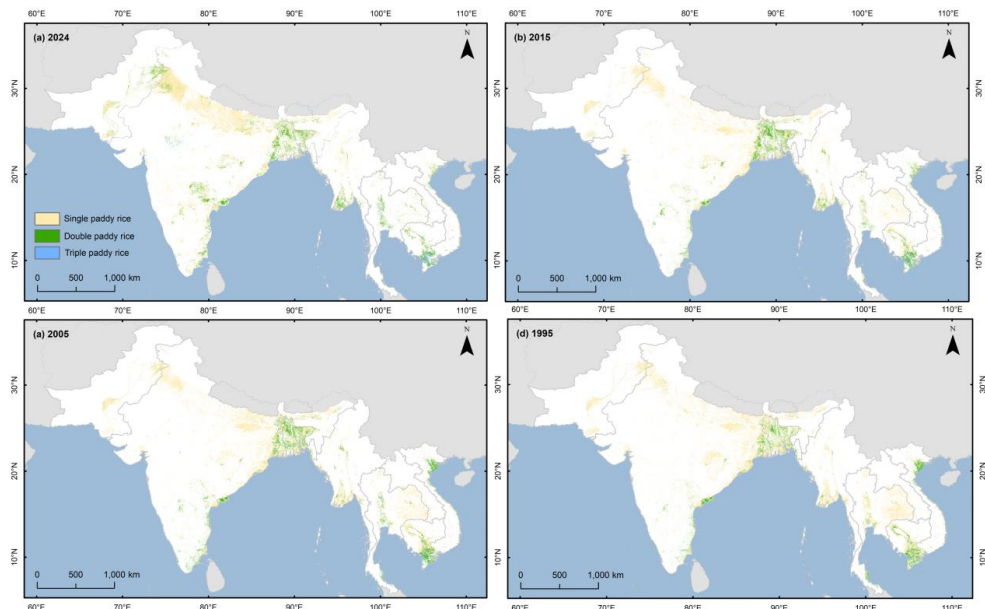
194 **3. Results**

195 **3.1 Validation of the spatial distribution accuracy of rice in South and mainland Southeast Asia**

196 The spatial distribution and cropping intensity of rice across South and mainland Southeast Asia are illustrated in
197 Fig. 2. The interactive version of this map can also be accessed and visualized using the GEE platform at: <https://ee-zhaozizhangcau.projects.earthengine.app/view/rice-planting-intensity--south--southeast-asia>.



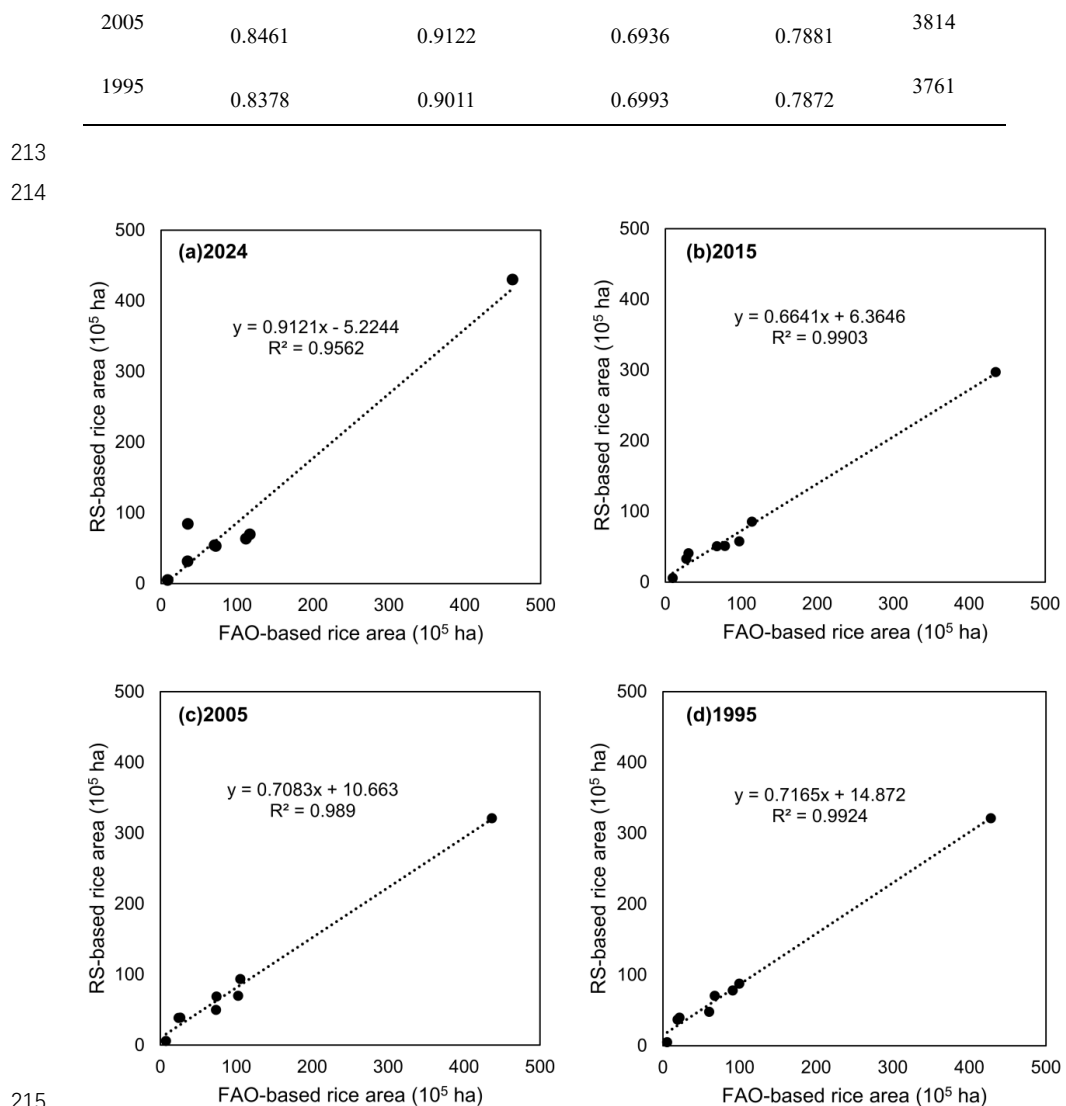
199 Based on validation using 23,396 sample points, the mapping accuracies for different years are summarized in
200 Table 3, with overall accuracies ranging from 83.74% to 87.60% and F1-scores between 0.7872 and 0.8628. The
201 2024 results achieved the highest accuracy, primarily because the higher temporal frequency of Sentinel-2
202 observations enabled more effective detection of flooding signals compared with the earlier Landsat sensors.
203 Mapping accuracies for other years did not show a declining trend over time, mainly due to the aggregation of
204 multi-year image archives and the use of biweekly composite imagery, which stabilized rice extraction
205 performance. Although Landsat-8 data were incorporated for the 2015 (2014–2016) period, residual striping
206 effects from Landsat-7 imagery slightly degraded the classification accuracy.
207



208
209 Figure 2. Long-term spatial distribution and planting intensity of rice in South and mainland Southeast Asia
210 (1995, 2005, 2015, 2024)
211

212 **Table 3** Accuracy assessment of paddy rice mapping results in South and Southeast Asia

Year	Overall Accuracy	User Accuracy	Producer Accuracy	F1 Score	Sample size
2024	0.8760	0.9668	0.7788	0.8628	8000
2015	0.8374	0.9500	0.7129	0.8143	7821



216 Figure 3. Comparison of RS-based rice area estimates with FAO statistics for South and mainland Southeast
217 Asia (1995, 2005, 2015, 2024)

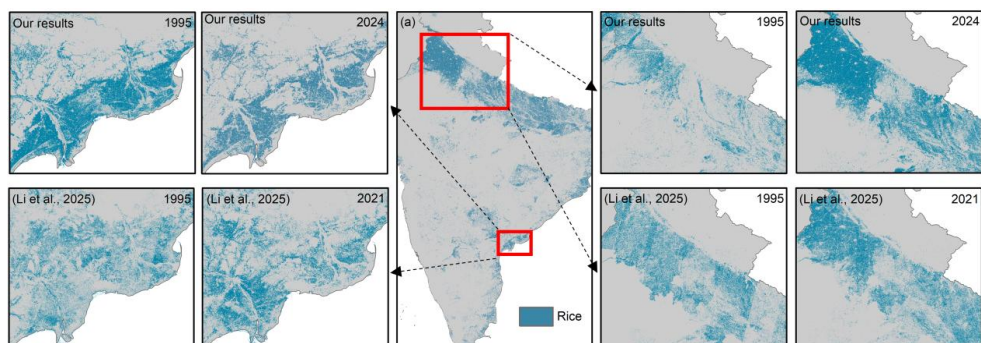
218 To further evaluate the accuracy of our results, we compared the estimated rice area from our generated rice
219 product with FAO statistical data (Fig. 2). The results showed that the R^2 values for all four years exceeded 0.9,
220 with a multi-year average RMSE of approximately 4.15 million hectares. Based on remote sensing retrievals, the
221 rice planting area across South and mainland Southeast Asian countries has increased by approximately 22.5
222 million hectares since the 1990s, with the largest increases observed in India and Bangladesh. Among these, the



223 2024 results exhibited the smallest discrepancy with statistical data. In Bangladesh, the remote sensing estimates
224 were relatively lower, potentially due to the influence of frequent flooding and cloud cover in the region.

225 **3.2 Comparison with other rice maps**

226 We selected typical rice-growing areas within the study region for visual comparison with other rice mapping
227 product. Specifically, in Vietnam, we compared our results with the land cover product (including rice layer)
228 released by JAXA. The spatial distributions were highly consistent across multiple years. In the 2005 results for
229 northern Vietnam, our product reduced some noise through image compositing and phenological identification
230 (Fig. S2). In the 2024 product for India, our results exhibited spatial distributions comparable to those of Li et al.
231 (2025) (Fig. 4). However, in the 1995 mapping of Punjab and other northern Indian provinces, Li's results were
232 notably affected by limited observation conditions, which manifested as strip-like artifacts in the output. By
233 contrast, our approach, which employed multi-year data compositing, effectively mitigated this issue. Differences
234 observed in the southeastern coastal regions of India further highlight the advantages of multi-year compositing
235 for rice mapping in the 1990s.

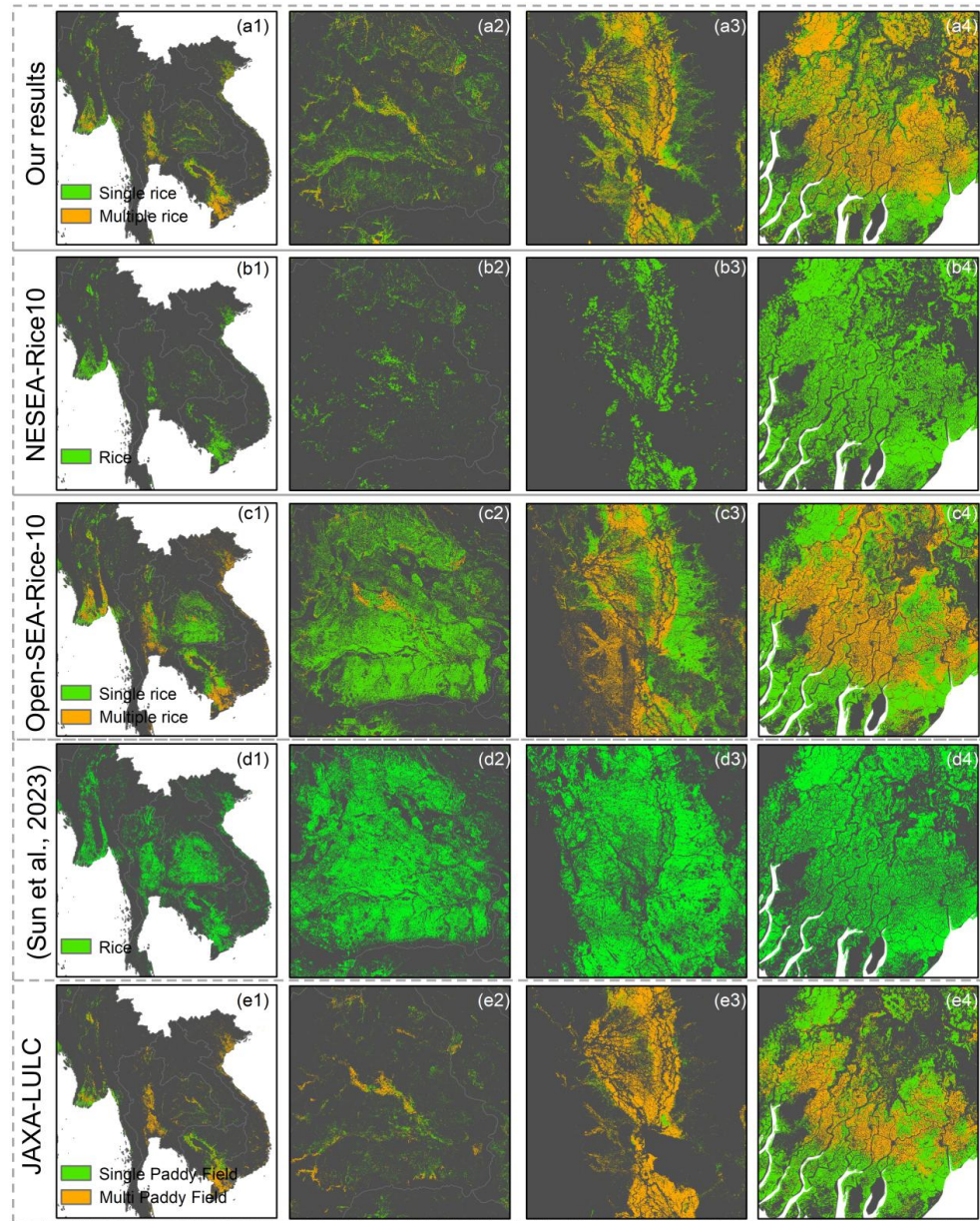


236
237 Figure 4. Comparison of rice distribution maps: Our Results compared to Li et al. (2025) for South Asia
238 (1995, 2021)
239

240 Notably, Fig. 5 presents a spatial comparison of five rice mapping products across Southeast Asia, including our
241 results. Among them, products a1, b1, and e1 exhibit relatively similar spatial distributions, whereas the NESEA-
242 Rice10 product captures the smallest rice extent. In contrast, c1 and d1 identified a greater number of rice pixels,
243 particularly in central–eastern Thailand, where both products detected extensive rice areas. We attribute these
244 differences mainly to the distinct responses of irrigated (paddy) and rainfed rice systems. The e2 panel, derived



245 from the JAXA LULC dataset, provides supporting evidence for this interpretation, as it delineates these regions
246 predominantly as paddy fields (see Section 4.1 for further discussion).
247 Panels a3–e3 illustrate the rice-growing regions in western Thailand, where three intensity-based products
248 consistently identified multi-season rice cultivation. However, the c3 product shows clear image boundary artifacts,
249 likely due to inconsistencies in image mosaicking. Spatially, the b3 product—derived from a single-year dataset—
250 identified a smaller extent of rice cultivation, while the d3 product appears to have overestimated rice coverage.
251 In contrast, along the moisture-rich coastal areas of Myanmar, all products exhibited relatively consistent spatial
252 patterns with minimal discrepancies.



253

254

255 Figure. 5 Comparative analysis of single and multiple rice field Distribution in Southeast Asia. Panels (a1)-

256 (a4) display results from our proposed method, (b1)-(b4) from NESEA-Rice10, (c1)-(c4) from Open-SEA-Rice-

257 10, and (d1)-(d4) from Sun et al. (2023). Panels (e1)-(e4) show JAXA-LULC data, retaining the original land

258 cover classifications of Single Paddy Field and Multi Paddy Field.



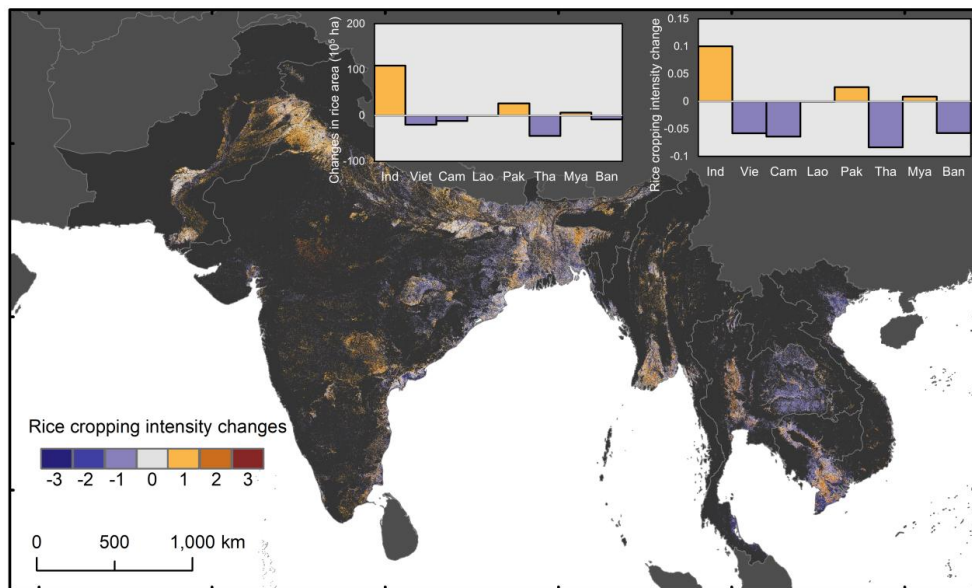
259 **3.3 Spatial patterns and change trends of rice cultivation over the past 30 years**

260 In South and mainland Southeast Asia, rice is predominantly distributed in plains and riverine areas with abundant
261 freshwater resources. Since 1990, there has been a significant expansion trend in rice planting areas, primarily in
262 central-western India and Pakistan (Fig. 2). Rice cropping intensity is dominated by double and single rice (this
263 study's statistics focus solely on rice cropping intensity, excluding other crops). The Mekong Delta region in
264 Vietnam is predominantly characterized by triple rice cultivation.

265 Based on the analysis of Figs. 2 and 6, substantial changes in rice cultivation patterns have occurred across South
266 and mainland Southeast Asia over the past three decades. In these regions, intensification within existing rice
267 croplands—manifested as increased planting intensity in stable areas—has become a more prevalent trend than
268 the expansion of rice-growing areas. For instance, regions previously dominated by single-cropping systems, such
269 as southern Thailand, have transitioned toward double-cropping regimes. Likewise, northern Pakistan and eastern
270 India have shown a pronounced increase in rice cropping intensity. In contrast, the Mekong Delta has experienced
271 a shift from double- to triple-cropping systems. Areas with reduced rice extent are primarily associated with
272 cropland degradation or conversion to other crops rather than a decline in planting intensity. The most notable
273 reductions are concentrated in eastern Thailand and the southern Mekong Delta estuary, corresponding
274 respectively to shifts from irrigated to rainfed systems and a loss of arable land.

275 As shown in Fig. 6, we further quantified changes in rice cultivation area and mean cropping intensity at the
276 national scale. Among all countries, India exhibited the most substantial expansion in rice cultivation area, whereas
277 most Southeast Asian countries experienced a general decline over the past three decades. In terms of cropping
278 intensity, India showed an average increase of approximately 0.1, while most Southeast Asian countries exhibited
279 a decrease of less than -0.05 , reflecting intensified cultivation in South Asia and widespread contraction in
280 Southeast Asia.

281



282

283

284

Figure 6. Spatial Distribution and Planting Intensity Changes of Paddy Rice in South and mainland Southeast Asia (1995–2024). Orange represents pixels with decreased paddy rice area in 2024 compared to 1995 (contraction), green indicates increased areas (expansion), and gray-white denotes stable areas (paddy rice present in both periods). Rice cropping intensity changes are shown for stable areas, with red indicating increases (+1 for one additional season, +2 for two additional seasons) and blue indicating decreases (-1 for one season less, -2 for two seasons less).

288

289 **4. Discussion**

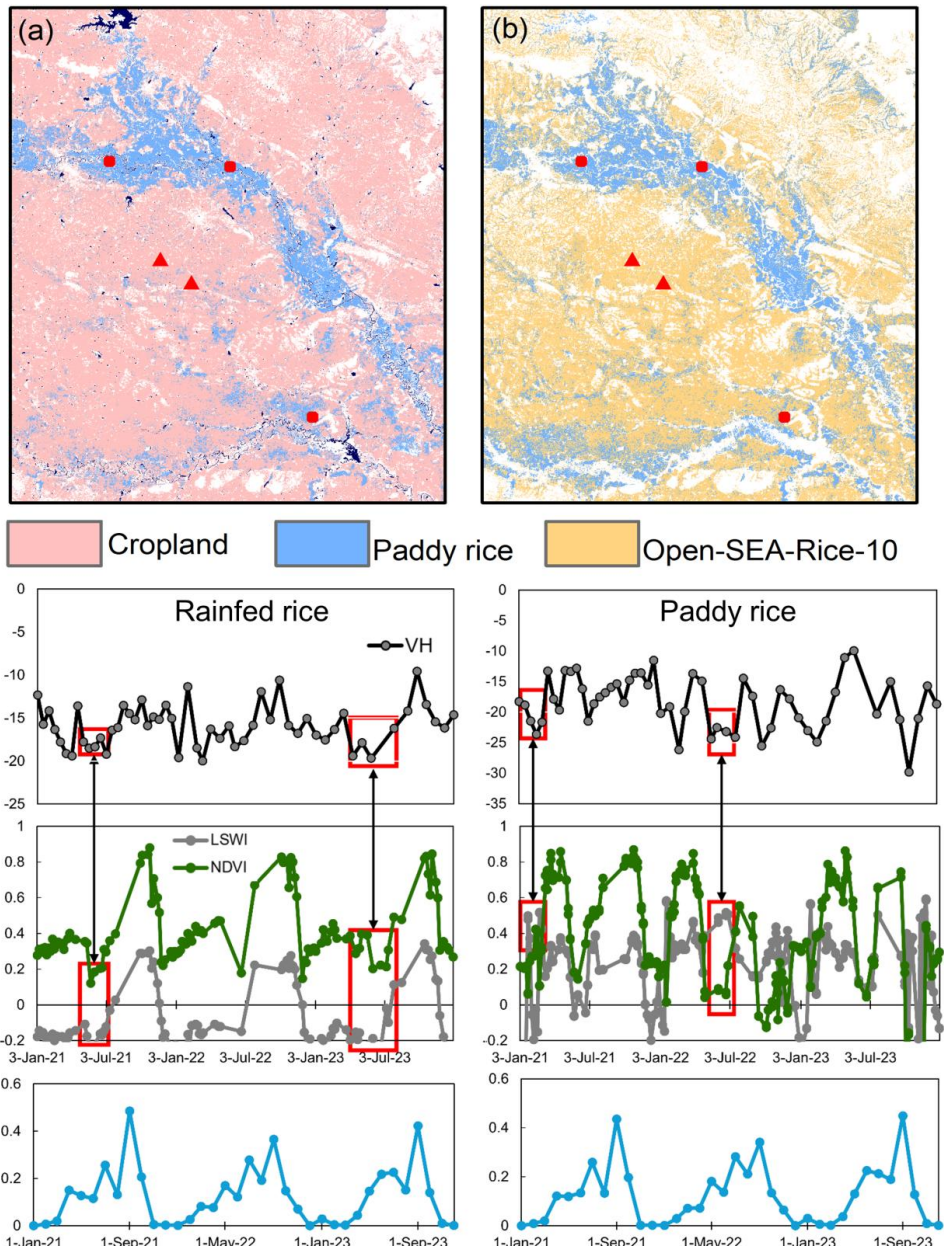
290 **4.1 Differences between Rainfed and Irrigated Rice**

291 In the results, substantial discrepancies among rice mapping products were observed in central–western Thailand.
292 To investigate the underlying causes, we analyzed the time-series profiles of selected sample points over three
293 consecutive years using the JAXA land-cover product, our phenology-based rice maps, and the Open-SEA-Rice-
294 10 dataset (Fig. 8).

295 From the optical time series, it is evident that rainfed rice fields do not maintain stable surface water coverage
296 during the “transplanting” stage. Consequently, they often fail to produce sufficiently low SWIR reflectance
297 relative to the RED band, which is required for satisfying the condition $LSWI \geq NDVI$ —the key indicator of
298 flooding used in phenology-based optical algorithms such as NESEA-Rice10. This explains why our optical-based



299 approach and other similar methods tend to identify fewer rice pixels compared with radar-based products shown
300 in Fig. 5.
301 By contrast, radar observations capture a distinct VH backscatter trough, indicating an increase in soil moisture
302 that alters the soil dielectric constant. As crop growth progresses, VH backscatter gradually rises, resulting in large
303 VH time series variations. This enables radar-based methods to detect rainfed rice, even in areas without persistent
304 standing water. Moreover, these VH minima typically coincide with the onset of the monsoon season, marking the
305 beginning of the rice growth cycle (Fig. 7).
306 For Irrigated rice, each valid cropping cycle is accompanied by a strong flooding signal that can be effectively
307 identified by all water-related optical indices (e.g., combinations of SWIR, RED, or GREEN bands; Zhao et al.
308 (2025)). In radar observations, paddy fields exhibit deeper VH troughs than rainfed fields, and the subsequent
309 increase after the trough (rice growing stage) reflects higher canopy water content (VWC) and a stronger dielectric
310 response, which amplifies VH time series variations. Unlike rainfed rice, the timing of Irrigated rice cultivation is
311 typically decoupled from monsoon onset, owing to irrigation management.
312 However, we also note a potential source of misclassification when relying solely on Sentinel-1 VH backscatter
313 for rice mapping, especially in temperate regions outside tropical zones. Although radar-based algorithms perform
314 well in persistently cloudy and humid environments, our previous findings—and those of other studies—indicate
315 that several non-rice crops (both rainfed and irrigated, such as maize and soybean) can exhibit amplitude variations
316 comparable to those of paddy rice (Zhao et al., 2024). Consequently, such V-shaped radar signatures are not unique
317 to rainfed or paddy rice, but rather represent a general biophysical response to canopy development and surface
318 moisture dynamics.



319
320 Figure 7. Spatial comparison and time-series analysis of vegetation indices, VH backscatter, and total
321 precipitation between rainfed and irrigated (paddy) rice in Thailand. (a) JAXA land-cover product, where pink
322 represents non-paddy croplands and blue indicates paddy fields. (b) Comparison between the Open-SEA-Rice-10



323 dataset (orange) and this study's paddy rice product (blue; overlaid on orange). The lower two panels present the
324 corresponding time-series curves for rainfed and paddy rice, respectively.

325 **4.2 Advantages of the proposed product**

326 Recent advances in remote sensing have produced numerous high-accuracy rice mapping algorithms (Deng et al.,
327 2025). However, their application to long-term, large-scale mapping remains constrained by data availability and
328 computational demands. For instance, although SAR can effectively improve mapping accuracy (Adrian et al.,
329 2021), its use is limited in earlier periods due to the absence of Sentinel-1 observations. In addition, the
330 computational complexity of large-scale mapping remains a considerable challenge, even when implemented on
331 cloud-based platforms such as Google Earth Engine.

332 To overcome these challenges, this study employs a streamlined and phenology-based rice mapping framework
333 specifically optimized for the biophysical and climatic conditions of South and Southeast Asia. Instead of
334 extracting detailed phenological phases (e.g., tillering or harvest), the method focuses on detecting key
335 phenological peaks, providing a robust solution under conditions of high cropping intensity, short intervals
336 between multiple rice cycles, and persistent monsoon-related cloud cover. For instance, in the Mekong Delta, the
337 interval between two consecutive rice seasons is perhaps shorter than 15 days (Fig. S3), meaning that even a slight
338 temporal offset in detecting the flooded transplanting stage could miss the short-lived flooding signal. Thus,
339 identifying phenological peaks offers a more reliable and practical strategy than full-season tracking using Landsat
340 imagery.

341

342 **4.2 Uncertainty Assessment**

343 The primary source of uncertainty or error in the products generated by this study stems from the observation
344 quality and the number of valid observations from the optical imagery data used. Specifically, the striping issue in
345 Landsat-7 data led to omission errors in some rice fields. Despite using all available imagery over a five-year
346 period for compositing, striped gaps persisted in certain areas, resulting in the failure to effectively identify rice
347 fields, particularly in the results for 2005 and 2015.

348 Additionally, validation based on sample points revealed omission errors in northern India, due to limitations in
349 valid optical observations. Based on the extracted rice phenological peaks, this region is characterized by a rice–
350 wheat double-cropping system, with rice transplanting typically occurring between June and July. However, as



351 shown in Fig. S4, many pixels in this region have very few valid observations during this period because of
352 persistent cloud cover. Consequently, optical imagery often fails to capture the flooding signals of rice, leading to
353 underestimation of rice extent and reduced accuracy in northern India.

354 To address this issue, we re-mapped the 2024 rice intensity and spatial distribution for northern India using our
355 previously developed Rice-Sentinel algorithm, which effectively integrates Sentinel-1 radar observations to
356 compensate for missing optical data. Nevertheless, the original optical-based results are also retained and provided
357 for comparison and reference by other researchers.

358

359 **5. Data availability**

360 The Spatial distribution and cropping intensity maps of rice in South and mainland Southeast Asia can be accessed
361 in the Zenodo data set from the following DOI: <https://doi.org/10.5281/zenodo.17615341> (Zhao et al., 2025b). We
362 welcome other researchers to validate these products and collaborate in improving the accuracy of rice mapping
363 in this region.

364 **6. Code availability**

365 The code independently developed of this study is available at the following link:
366 <https://code.earthengine.google.com/d410ce31604e93518ef9281097e71cc5>.

367 **7. Conclusions**

368 This study employed an improved phenology-based rice mapping algorithm, leveraging the full archive of Landsat
369 series and Sentinel-2 satellite data, to generate high-resolution maps of rice planting areas and cropping intensity
370 across South and mainland Southeast Asia for the years 1995, 2005, 2015, and 2024. By applying optical image
371 compositing and a fake-peak filtering technique, the challenges of extracting long-term rice cropping intensity in
372 tropical regions were effectively addressed, yielding relatively reliable results. The resulting products achieved
373 overall accuracies ranging from 83.74% to 87.60% across the four periods, validated against 23,396 independent
374 samples, and exhibited R^2 values exceeding 0.9 when compared with FAO statistical data for South and mainland
375 Southeast Asian countries. In conclusion, this study fills a critical gap in high-resolution, long-term rice mapping.



376 providing a robust foundation for sustainable agricultural practices and policy development in South and Southeast
377 Asia, with broader implications for global food security and environmental sustainability.

378 **References**

379 Adrian, J., Sagan, V., and Maimaitijiang, M.: Sentinel SAR-optical fusion for crop type mapping using deep
380 learning and Google Earth Engine, ISPRS Journal of Photogrammetry and Remote Sensing, 175, 215-235,
381 <https://doi.org/10.1016/j.isprsjprs.2021.02.018>, 2021.

382 Carrasco, L., Fujita, G., Kito, K., and Miyashita, T.: Historical mapping of rice fields in Japan using phenology
383 and temporally aggregated Landsat images in Google Earth Engine, ISPRS Journal of Photogrammetry and
384 Remote Sensing, 191, 277-289, <https://doi.org/10.1016/j.isprsjprs.2022.07.018>, 2022.

385 Chen, Z., Balasus, N., Lin, H., Nesser, H., and Jacob, D. J.: African rice cultivation linked to rising methane, Nature
386 Climate Change, 14, 148-151, 10.1038/s41558-023-01907-x, 2024.

387 Deng, Y., Peng, B., Guan, K., Runkle, B. R. K., Moreno-García, B., Wu, X., Wang, S., Zhou, Q., and Reba, M. L.:
388 Detecting the onset of rice field inundation in the Lower Mississippi River Basin via Harmonized Landsat Sentinel-
389 2 (HLS) satellite time series, ISPRS Journal of Photogrammetry and Remote Sensing, 228, 28-43,
390 <https://doi.org/10.1016/j.isprsjprs.2025.07.003>, 2025.

391 Dong, J. and Xiao, X.: Evolution of regional to global paddy rice mapping methods: A review, ISPRS Journal of
392 Photogrammetry and Remote Sensing, 119, 214-227, <https://doi.org/10.1016/j.isprsjprs.2016.05.010>, 2016.

393 Dong, J., Xiao, X., Menarguez, M. A., Zhang, G., Qin, Y., Thau, D., Biradar, C., and Moore, B.: Mapping paddy
394 rice planting area in northeastern Asia with Landsat 8 images, phenology-based algorithm and Google Earth
395 Engine, Remote Sensing of Environment, 185, 142-154, <https://doi.org/10.1016/j.rse.2016.02.016>, 2016.

396 Dong, J., Xiao, X., Kou, W., Qin, Y., Zhang, G., Li, L., Jin, C., Zhou, Y., Wang, J., Biradar, C., Liu, J., and Moore,
397 B.: Tracking the dynamics of paddy rice planting area in 1986–2010 through time series Landsat images and
398 phenology-based algorithms, Remote Sensing of Environment, 160, 99-113,
399 <https://doi.org/10.1016/j.rse.2015.01.004>, 2015.

400 Foley, J. A., DeFries, R., Asner, G. P., Barford, C., Bonan, G., Carpenter, S. R., Chapin, F. S., Coe, M. T., Daily,
401 G. C., Gibbs, H. K., Helkowski, J. H., Holloway, T., Howard, E. A., Kucharik, C. J., Monfreda, C., Patz, J. A.,
402 Prentice, I. C., Ramankutty, N., and Snyder, P. K.: Global Consequences of Land Use, Science, 309, 570-574,
403 10.1126/science.1111772, 2005.

404 Gao, Y., Pan, Y., Zhu, X., Li, L., Ren, S., Zhao, C., and Zheng, X.: FARM: A fully automated rice mapping
405 framework combining Sentinel-1 SAR and Sentinel-2 multi-temporal imagery, Computers and Electronics in
406 Agriculture, 213, 108262, <https://doi.org/10.1016/j.compag.2023.108262>, 2023.

407 Ge, J., Zhang, H., Zuo, L., Xu, L., Jiang, J., Song, M., Ding, Y., Xie, Y., Wu, F., Wang, C., and Huang, W.: Large-
408 scale rice mapping under spatiotemporal heterogeneity using multi-temporal SAR images and explainable deep
409 learning, ISPRS Journal of Photogrammetry and Remote Sensing, 220, 395-412,
410 <https://doi.org/10.1016/j.isprsjprs.2024.12.021>, 2025.

411 Ginting, F. I., Rudiyanto, R., Fatchurrahman, Mohd Shah, R., Che Soh, N., Eng Giap, S. G., Fiantis, D., Setiawan,
412 B. I., Schiller, S., Davitt, A., and Minasny, B.: High-resolution maps of rice cropping intensity across Southeast
413 Asia, Scientific Data, 12, 1408, 10.1038/s41597-025-05722-1, 2025.

414 Godfray, H. C. J., Beddington, J. R., Crute, I. R., Haddad, L., Lawrence, D., Muir, J. F., Pretty, J., Robinson, S.,
415 Thomas, S. M., and Toulmin, C.: Food Security: The Challenge of Feeding 9 Billion People, 327, 812-818,
416 doi:10.1126/science.1185383, 2010.



417 Han, J., Zhang, Z., Luo, Y., Cao, J., Zhang, L., Cheng, F., Zhuang, H., Zhang, J., and Tao, F.: NESEA-Rice10:
418 high-resolution annual paddy rice maps for Northeast and Southeast Asia from 2017 to 2019, *Earth Syst. Sci. Data*,
419 13, 5969-5986, 10.5194/essd-13-5969-2021, 2021.

420 Han, J., Zhang, Z., Luo, Y., Cao, J., Zhang, L., Zhuang, H., Cheng, F., Zhang, J., and Tao, F.: Annual paddy rice
421 planting area and cropping intensity datasets and their dynamics in the Asian monsoon region from 2000 to 2020,
422 *Agricultural Systems*, 200, 103437, <https://doi.org/10.1016/j.agsy.2022.103437>, 2022.

423 He, Y., Dong, J., Liao, X., Sun, L., Wang, Z., You, N., Li, Z., and Fu, P.: Examining rice distribution and cropping
424 intensity in a mixed single- and double-cropping region in South China using all available Sentinel 1/2 images,
425 *International Journal of Applied Earth Observation and Geoinformation*, 101, 102351,
426 <https://doi.org/10.1016/j.jag.2021.102351>, 2021.

427 Huang, H., Wang, J., Liu, C., Liang, L., Li, C., and Gong, P.: The migration of training samples towards dynamic
428 global land cover mapping, *ISPRS Journal of Photogrammetry and Remote Sensing*, 161, 27-36,
429 <https://doi.org/10.1016/j.isprsjprs.2020.01.010>, 2020.

430 Karra, K., Kontgis, C., Statman-Weil, Z., Mazzariello, J. C., Mathis, M., and Brumby, S. P.: Global land use / land
431 cover with Sentinel 2 and deep learning, 2021 IEEE International Geoscience and Remote Sensing Symposium
432 IGARSS, 11-16 July 2021, 4704-4707, 10.1109/IGARSS47720.2021.9553499,

433 Li, S., Shen, R., Jiang, J., Peng, Q., Chen, X., Dong, J., Dong, J., and Yuan, W.: A long-term paddy rice distribution
434 dataset in Asia at a 30 m spatial resolution, *Scientific Data*, 12, 1052, 10.1038/s41597-025-05374-1, 2025.

435 Lin, Z., Zhong, R., Xiong, X., Guo, C., Xu, J., Zhu, Y., Xu, J., Ying, Y., Ting, K. C., Huang, J., and Lin, T.: Large-
436 Scale Rice Mapping Using Multi-Task Spatiotemporal Deep Learning and Sentinel-1 SAR Time Series, 14, 699,
437 2022.

438 Mehta, P., Siebert, S., Kummu, M., Deng, Q., Ali, T., Marston, L., Xie, W., and Davis, K. F.: Half of twenty-first
439 century global irrigation expansion has been in water-stressed regions, *Nature Water*, 2, 254-261, 10.1038/s44221-
440 024-00206-9, 2024.

441 Ni, R., Tian, J., Li, X., Yin, D., Li, J., Gong, H., Zhang, J., Zhu, L., and Wu, D.: An enhanced pixel-based
442 phenological feature for accurate paddy rice mapping with Sentinel-2 imagery in Google Earth Engine, *ISPRS
443 Journal of Photogrammetry and Remote Sensing*, 178, 282-296, <https://doi.org/10.1016/j.isprsjprs.2021.06.018>,
444 2021.

445 Persaud, N. and Dagher, R.: The United Nations: 2030 Sustainable Development Goals Agenda, in: *The Role of
446 Monitoring and Evaluation in the UN 2030 SDGs Agenda*, edited by: Persaud, N., and Dagher, R., Springer
447 International Publishing, Cham, 1-41, 10.1007/978-3-030-70213-7_1, 2021.

448 Potapov, P., Turubanova, S., Hansen, M. C., Tyukavina, A., Zalas, V., Khan, A., Song, X.-P., Pickens, A., Shen,
449 Q., and Cortez, J.: Global maps of cropland extent and change show accelerated cropland expansion in the twenty-
450 first century, *Nature Food*, 3, 19-28, 10.1038/s43016-021-00429-z, 2022.

451 Singha, M., Dong, J., Zhang, G., and Xiao, X.: High resolution paddy rice maps in cloud-prone Bangladesh and
452 Northeast India using Sentinel-1 data, *Scientific Data*, 6, 26, 10.1038/s41597-019-0036-3, 2019.

453 Song, M., Xu, L., Ge, J., Zhang, H., Zuo, L., Jiang, J., Ding, Y., Xie, Y., and Wu, F.: EARice10: a 10 m resolution
454 annual rice distribution map of East Asia for 2023, *Earth Syst. Sci. Data*, 17, 661-683, 10.5194/essd-17-661-2025,
455 2025.

456 Sun, C., Zhang, H., Xu, L., Ge, J., Jiang, J., Zuo, L., and Wang, C.: Twenty-meter annual paddy rice area map for
457 mainland Southeast Asia using Sentinel-1 synthetic-aperture-radar data, *Earth Syst. Sci. Data*, 15, 1501-1520,
458 10.5194/essd-15-1501-2023, 2023.

459 Thorp, K. R. and Drajat, D.: Deep machine learning with Sentinel satellite data to map paddy rice production
460 stages across West Java, Indonesia, *Remote Sensing of Environment*, 265, 112679,



461 <https://doi.org/10.1016/j.rse.2021.112679>, 2021.

462 Wang, Y., Hollingsworth, P. M., Zhai, D., West, C. D., Green, J. M. H., Chen, H., Hurni, K., Su, Y., Warren-Thomas,
463 E., Xu, J., and Ahrends, A.: High-resolution maps show that rubber causes substantial deforestation, *Nature*, 623,
464 340-346, 10.1038/s41586-023-06642-z, 2023.

465 Xiao, X., Boles, S., Frolking, S., Li, C., Babu, J. Y., Salas, W., and Moore, B.: Mapping paddy rice agriculture in
466 South and Southeast Asia using multi-temporal MODIS images, *Remote Sensing of Environment*, 100, 95-113,
467 <https://doi.org/10.1016/j.rse.2005.10.004>, 2006.

468 Xiao, X., Boles, S., Liu, J., Zhuang, D., Frolking, S., Li, C., Salas, W., and Moore, B.: Mapping paddy rice
469 agriculture in southern China using multi-temporal MODIS images, *Remote Sensing of Environment*, 95, 480-
470 492, <https://doi.org/10.1016/j.rse.2004.12.009>, 2005.

471 Xu, S., Zhu, X., Chen, J., Zhu, X., Duan, M., Qiu, B., Wan, L., Tan, X., Xu, Y. N., and Cao, R.: A robust index to
472 extract paddy fields in cloudy regions from SAR time series, *Remote Sensing of Environment*, 285, 113374,
473 <https://doi.org/10.1016/j.rse.2022.113374>, 2023.

474 Yang, J., Dong, J., Liu, L., Zhao, M., Zhang, X., Li, X., Dai, J., Wang, H., Wu, C., You, N., Fang, S., Pang, Y., He,
475 Y., Zhao, G., Xiao, X., and Ge, Q.: A robust and unified land surface phenology algorithm for diverse biomes and
476 growth cycles in China by using harmonized Landsat and Sentinel-2 imagery, *ISPRS Journal of Photogrammetry*
477 and *Remote Sensing*, 202, 610-636, <https://doi.org/10.1016/j.isprsjprs.2023.07.017>, 2023.

478 Zabel, F., Delzeit, R., Schneider, J. M., Seppelt, R., Mauser, W., and Václavík, T.: Global impacts of future cropland
479 expansion and intensification on agricultural markets and biodiversity, *Nature Communications*, 10, 2844,
480 10.1038/s41467-019-10775-z, 2019.

481 Zeng, Z., Estes, L., Ziegler, A. D., Chen, A., Searchinger, T., Hua, F., Guan, K., Jintrawet, A., and F. Wood, E.:
482 Highland cropland expansion and forest loss in Southeast Asia in the twenty-first century, *Nature Geoscience*, 11,
483 556-562, 10.1038/s41561-018-0166-9, 2018.

484 Zhan, P., Zhu, W., and Li, N.: An automated rice mapping method based on flooding signals in synthetic aperture
485 radar time series, *Remote Sensing of Environment*, 252, 112112, <https://doi.org/10.1016/j.rse.2020.112112>, 2021.

486 Zhang, G., Xiao, X., Dong, J., Xin, F., Zhang, Y., Qin, Y., Doughty, R. B., and Moore, B.: Fingerprint of rice
487 paddies in spatial – temporal dynamics of atmospheric methane concentration in monsoon Asia, *Nature
488 Communications*, 11, 554, 10.1038/s41467-019-14155-5, 2020.

489 Zhang, G., Xiao, X., Biradar, C. M., Dong, J., Qin, Y., Menarguez, M. A., Zhou, Y., Zhang, Y., Jin, C., Wang, J.,
490 Doughty, R. B., Ding, M., and Moore, B.: Spatiotemporal patterns of paddy rice croplands in China and India from
491 2000 to 2015, *Science of The Total Environment*, 579, 82-92, <https://doi.org/10.1016/j.scitotenv.2016.10.223>,
492 2017.

493 Zhang, X., Liu, L., Chen, X., Gao, Y., Xie, S., and Mi, J.: GLC_FCS30: global land-cover product with fine
494 classification system at 30 m using time-series Landsat imagery, *Earth Syst. Sci. Data*, 13, 2753-2776,
495 10.5194/essd-13-2753-2021, 2021.

496 Zhao, Z., Dong, J., Zhang, G., Yang, J., Liu, R., Wu, B., and Xiao, X.: Improved phenology-based rice mapping
497 algorithm by integrating optical and radar data, *Remote Sensing of Environment*, 315, 114460,
498 <https://doi.org/10.1016/j.rse.2024.114460>, 2024.

499 Zhao, Z., Dong, J., Yang, J., Liu, L., You, N., Xiao, X., and Zhang, G.: From rice planting area mapping to rice
500 agricultural system mapping: A holistic remote sensing framework for understanding China's complex rice systems,
501 *ISPRS Journal of Photogrammetry and Remote Sensing*, 224, 382-397,
502 <https://doi.org/10.1016/j.isprsjprs.2025.03.026>, 2025a.

503 Zhao, Z., Dong, J., Zhang, G., Yang, J., and Xiao, X.: Mapping Paddy Rice Distribution and Cropping Intensity in
504 South and Southeast Asia (1995 - 2024) at 30m Resolution, <https://doi.org/10.5281/ZENODO.17615341>, 2025b.